Effects of the local mechanical environment on vertebrate tissue differentiation during repair: does repair recapitulate development?

Dennis M. Cullinane[1,3,*], Kristy T. Salisbury[1,3], Yaser Alkhiary[2], Solomon Eisenberg[3],
Louis Gerstenfeld[1] and Thomas A. Einhorn[1]

[1]*Orthopaedic Research Laboratory, Department of Orthopaedic Surgery, Boston University Medical Center, 715
Albany Street, Housman-205, Boston, MA 02118-2526, USA,* [2]*Department of Restorative Sciences and Biomaterials,
Boston University School of Dental Medicine, Boston, MA 02118, USA* and [3]*Department of Biomedical Engineering,
Boston University, Boston, MA 02115, USA*

*Author for correspondence (e-mail: bones@bu.edu)

Summary

The local mechanical environment is a crucial factor in determining cell and tissue differentiation during vertebrate skeletal development and repair. Unlike the basic response of bone to mechanical load, as described in Wolff's law, the mechanobiological relationship between the local mechanical environment and tissue differentiation influences everything from tissue type and molecular architecture to the formation of complex joints. This study tests the hypothesis that precisely controlled mechanical loading can regulate gene expression, tissue differentiation and tissue architecture in the adult skeleton and that precise manipulation of the defect's local mechanical environment can initiate a limited recapitulation of joint tissue development. We generated tissue type predictions using finite element models (FEMs) interpreted by published mechanobiological fate maps of tissue differentiation. The experiment included a custom-designed external fixator capable of introducing daily bending, shear or a combination of bending and shear load regimens to induce precisely controlled mechanical conditions within healing femoral defects. Tissue types and ratios were characterized using histomorphometrics and molecular markers. Tissue molecular architecture was quantified using polarized light and Fourier transforms, while immunological staining and *in situ* hybridization were used to characterize gene expression. The finite element models predicted the differentiation of cartilage within the defects and that substantial fibrous tissues would develop along the extreme excursion peripheries in the bending group. The three experimentally induced loading regimens produced contiguous cartilage bands across all experimental defects, inhibiting bony healing. Histomorphometric analysis of the ratios of cartilage to bone in the experimental groups were not significantly different from those for the knee joint, and Fourier transform analysis determined significantly different collagen fibril angle specializations within superficial, intermediate and deep layers of all experimental cartilages ($P<0.0001$), approximating those for articular cartilage. All stimulations resulted in the expression of collagen type II, while the bending stimulation also resulted in the expression of the joint-determining gene *GDF-5*. These findings indicate that the local mechanical environment is an important regulator of gene expression, tissue differentiation and tissue architecture.

Key words: local mechanical environment, mechanical loading, mechanobiology, tissue differentiation, tissue architecture, gene expression, finite element model, skeleton, cartilage, bone.

Introduction

Mechanobiology, a science that relates mechanical loading history to every level of tissue formation from genetic expression and tissue differentiation to tissue architecture and mechanical properties, has shown great promise in furthering our understanding of tissue development, ontological adaptation and repair. Its roots date back to the work of Wolff (1892), who suggested that the daily mechanical environment will influence the gross morphology of skeletal tissue architecture. Recent models of the local mechanical environment within skeletal tissues suggest that this phenomenon plays a crucial role in creating, maintaining or repairing the skeleton (Beaupre et al., 2000; Carter and Beaupre, 2001; Carter, 1987; Carter et al., 1991; Cullinane et al., 1999, 2002; van der Meulen et al., 1993, 1995; van der Meulen and Huiskes, 2001; Whalen, 1993). Mechanical stability has likewise been shown to influence revascularization within a healing defect (Claes et al., 2002), a necessary stage in the formation of new bone tissues.

However, aside from simple changes in tissue architecture, this mechanosensitivity of the skeleton is also likely to include a direct influence on gene expression, tissue molecular architecture and tissue type during the processes of development and healing (Carter et al., 1998a,b; Claes and Heigele, 1999; Claes et al., 2002; Cullinane et al., 1999, 2002; Hartman and Tabin, 2001; Elder et al., 2001; Gardner et al., 2000; Loboa et al., 2001; Smith-Adaline et al., 2002; Waanders et al., 1998). In fact, several studies have made direct parallels between joint development and fracture repair based on this relationship (Cullinane et al., 2002; Ferguson et al., 1999). Thus, not only does the mechanical environment initiate tissue formation and resorption due to exercise and disuse, for example, but it can also regulate the very type of tissue that will form during development or healing.

Appropriate mechanical stimulation is essential in directing complex tissue differentiation and architecture during joint development (Carter et al., 1998b; Eckstein et al., 2002; Heegaard et al., 1999; Sarin and Carter, 2000; Smith et al., 1992; van der Meulen and Carter, 1995), and the mechanical properties of the resulting tissues can be correlated to the applied load (Grodzinsky et al., 2000). Thus, cartilage, and specifically articular cartilage, demonstrates direct dependence on the mechanical environment for normal development and maintenance (Beaupre et al., 2000; Grodzinsky et al., 2000; Loboa-Polefka et al., 2002). Evidence of this relationship can be found in studies of joint immobilization in which the absence of mechanical loading significantly alters tissue developmental pathways even in developmentally predetermined joint tissues (de Rooji et al., 2001; Hall, 1972; Smith et al., 1992). In this way, the mechanical environment can specifically foster cartilage formation instead of bone or fibrous tissues, and it can regulate the architecture of those tissues down to their molecular configuration (Cullinane et al., 2002).

The model

This study was designed to empirically test the mechanobiological paradigm as it applies to gene expression, tissue differentiation and tissue architecture in a healing skeletal defect. The goal of this experimental design was to mimic the local mechanical environment during early joint development (post-segmentation) using a custom-designed external fixation device capable of inducing bending and shear loads within a healing bone defect. Finite element models (FEMs) generate estimates of stress and strain distributions within the defects that are then used to predict tissue type and distribution based on a mechanobiologically derived tissue differentiation fate map (MFM) based on Carter et al. (1988).

Materials and methods
Finite element models

Finite element models (FEMs) were used to predict development of specific tissue types and their spatial distribution within the defect in response to each mechanical
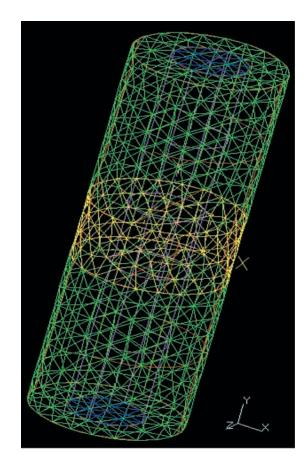

Fig. 1. A finite element model of the defect. Cortical bone is represented as an ideal tube of appropriate thickness, while the defect is represented as a mid-segment of the tube. The mechanical properties of the defect tissues are taken from the literature for callus mechanics, while the cortical bone is modeled as an incompressible solid. The model incorporates geometry, mechanical properties and load characteristics and generates stress and strain distribution fields that are used to create tissue differentiation predictions.

treatment. Predictions of tissue compositions required a representative three-dimensional reconstruction of the defect based on applied input loads and tissue material properties (Fig. 1). The FEMs generated estimates of experimentally imposed stress and strain distributions within the modeled defect. These models were based on a bone defect FEM by Carter et al. (1988), using ideal geometric tubes to represent the femur and a mid-tube segment to represent the defect.

The cortical bone of the femoral diaphysis served as a rigid boundary because the bone is several orders of magnitude stiffer than the materials within the early healing defect. The defect is represented by a middle segment of the tube with different mechanical properties from the cortical bone portion of the tube and the medullary canal. Values for the mechanical properties of the defect tissues were taken from the literature for an equivalent early stage of maturation (Gardner et al., 2000). It was expected that the early callus would be representative of a fluid to semi-solid phase material with hydrostatic forces dominating. The bending and shear models

were used to (1) estimate local mechanical loading conditions and, using that information, to (2) predict the patterns of tissue differentiation within the defect.

The FEM is comprised of a number of nodes and brick elements. We estimated the brick elements to be 0.05 mm in magnitude. The FE analysis was performed using I-DEAS software (Schroff Development Corp., Mission, KS, USA). Solids including bone and condensed cell masses were meshed into elements using mesh generation software. Stress and strain distributions were estimated by the FEMs, and tissue types were assigned based on a mechanobiologically derived tissue differentiation fate map (MFM) based on Carter et al. (1988, 1998a,b). Hydrostatic stress and maximum principal tensile strain were calculated for the different mechanical actions, and spatial tissue predictions were assigned based upon quantitative, as well as relative, stress and strain levels according to Giori et al. (1993). The tissue types we predicted based on our mechanical stimulations included cartilage (under relatively high hydrostatic compressive stress), fibrocartilage (under relatively high hydrostatic stress and high tensile strain), bone (under relatively low hydrostatic stress and low hydrostatic strain) and fibrous tissue (under relatively low hydrostatic stress but high tensile strain).

External fixation

A total of twelve Sprague–Dawley rats (*Rattus norvegicus* Berkkenhaut 1769) weighing 421 ± 34 g were used in this study. Animal care and experimental protocols were followed in accordance with NIH guidelines and approved by our institution's Animal Care and Use Committee. Four animals were used in each of the groups that were subjected to bending, shear or alternating bending and shear. The external fixator was modified from a previous model, while the surgical procedure was identical to that used in a previous report from our laboratory (Cullinane et al., 2002). Briefly, the external fixator was surgically applied to the right femur using four bicortical pins, and an osteotomy was created leaving a 2 mm defect within the femoral diaphysis. The external fixator, in conjunction with the linkage system, was capable of imposing either 12° symmetrical bending or 10% symmetrical cortical shear, depending on the actuator pin insertion configuration (Fig. 2A). The fixator body was composed of two articulating solid aluminum rectangular prisms with cortical pin holes and included clamping and locking screws. The clamping screws fastened the cortical pins into the fixator, and the locking screws arrested the fixator pivot or shear actions (Fig. 2B).

Mechanical stimulation

The stimulation protocol followed that established for a previous study from our laboratory (Cullinane et al., 2002). To perform the mechanical stimulations, an oscillating linkage system was built that supplied a rotational moment that could be applied to the fixators as an oscillating vertical displacement (Fig. 3). The vertical displacement was translated by the fixator into either 10% shear or 12° bending. The action was applied
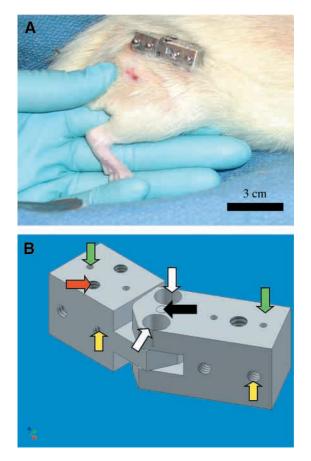

Fig. 2. An external fixator mounted on a rat femur with an AutoCad representation of the device. (A) The pin clamping screws can be seen facing out from the animal. The device is in the straight and locked position, maintaining rigid fixation within the defect. The healed surgical incision site can be seen below the fixator. (B) The bicortex pins are situated in the pin channels (green arrows) and are fixed by clamp screws (yellow arrows). The black arrow indicates the axis of the bending fixator. When the locking screws are in place (white arrows), the device is capable of rigid fixation.

using a servomotor (model #2602-010, QCI-23-5-E-01; Quicksilver Controls Inc., Covina, CA, USA). The speed of the motor was controlled using PC-based software. The shaft of the servomotor was coupled to one of two eccentric shafts of a torque transducer (model #1102-50; Lebow Products, Troy, MI, USA). The other shaft of the transducer was connected to the linkage system. A torque sensor incorporated within the system was connected to an external data acquisition board (model #100; InstruNet Inc., Cambridge, MA, USA) and acted as a bridge voltage sensor, measuring the torque transduced to the fixator. Based on the manufacturer's specifications, the torque sensor was mapped to 278.6 mV Nm^{-1}, with the input torque sampled at 60 Hz for the duration of each experimental session. The peak torque required to induce the respective motions prior to animal attachment was recorded as the baseline value. The loading apparatus was calibrated prior to every application using InstruNet and Quicksilver PC-based software.

There were three mechanical stimulation protocols executed during this study: (1) bending at 12°, (2) 10% shear and (3) alternating 12° bending and 10% shear (percentage of cortex diameter). All mechanical stimulations were symmetrical to the alignment of the cortices and cyclical for the 15-min stimulation period. Starting at post-operative day three and continuing for six weeks, the mechanical stimulations were induced for six consecutive days, with one day of rest each week. The fixator on each animal was attached to the linkage system that instituted the respective bending and shear actions initiated by the motor. The results from these three treatment groups were compared with those of previous control specimens.

During each mechanical session, the treatment animals were anesthetized, the fixators were attached to the linkage, the locking screws were removed, and cyclic stimulations were applied for 15 min at a frequency of 1 Hz. A dedicated computer coordinated the application of the mechanical treatment and data acquisition during calibration and treatment. The locking screws were replaced upon completion of each session. Once recovered from the anesthesia, the animals were returned to the housing room and allowed to ambulate freely in their cages.

Moment analysis

A torque sensor incorporated within the system was connected to an external data acquisition board (model #100; InstruNet Inc.) and acted as a bridge voltage sensor, measuring the torque transduced to the fixator and the resistance to the applied torque. Based on the manufacturer's specifications, the torque sensor was mapped to 278.6 mV Nm^{-1}, with the input torque sampled at 60 Hz for the duration of each experimental
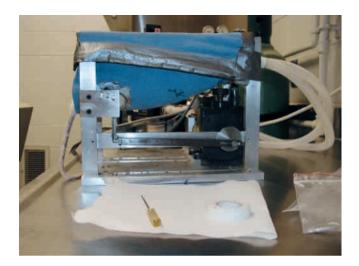

Fig. 3. The linkage system connecting the motor and torque sensor to the fixator, which is inserted by pins into the rat femur. As the wheel (bottom right) rotates, the horizontal actuator arm (bottom) drives the vertical accuator arm (bottom left), which is attached to one side of the fixator (hidden by the plate). As the fixator bends on its axis or displaces in shear, the defect is stimulated. The rat is lying in a sling hammock with its tail protruding to the left of the image.

session. The loading apparatus was calibrated prior to every application using InstruNet and Quicksilver PC-based software. The peak torque required to induce the respective motions prior to animal attachment was recorded as the baseline value. The torque sensor then constantly monitored the torsional resistance to the motor *via* the skeletal defect within the animal. These resistance data were captured for each animal during every daily stimulation period, the data were then averaged among all the animals for every day of stimulation, and the result was a mean daily moment resistance for every day of the stimulation protocol. The mean relative moment resistance was charted for the entire 35-day stimulation period.

Histology

Animals were euthanized at the termination of the study and the femora were excised. Standard histological methods were employed to generate serial 5 μm sagittal sections for standard histology and histomorphometry (Cullinane et al., 2002). The sections were mounted on glass slides, and even-numbered slides were stained using Safranin-O (cartilage) and Fast Green (bone), while odd-numbered slides were stained with Alcian Blue and counter-stained with eosin (proteoglycans). The 5 μm decalcified histological specimens were examined under a light microscope using 1.25× to 40× objectives. Dark-field images were obtained through the use of a polarizing filter, which highlighted collagen fibrils for quantification of their orientation and conformity within the extracellular matrix.

Histomorphometrics

Tissue type composition

Tissue type area composition was quantified using ImagePro® software (Atlanta, GA, USA). We quantified the percentage of bone and cartilage for each of the treatment groups and the control group, as well as rat knee and lumbar intervertebral joints. The entire defect and joint were quantified for tissue percentage within a standardized area of interest, including 2.5 mm in both directions proximal and distal to the defect or joint center. Tissue type ratios were generated for each treatment group and the controls, as well as actual native rat joints. Comparisons were made to identify similarities in tissue composition ratios between the treatment groups and the native rat joints.

Collagen architecture quantification

In order to characterize the molecular organization of the newly formed cartilage tissues, collagen fibril orientation and angular agreement were quantified using polarizing light microscopy and histomorphometric analyses using Matlab® and ImagePro®. Fast Fourier transforms were performed on digitized images of polarized light micrographs, and the preferred collagen fibril orientation was determined by the most intense region in their power spectra (Fig. 4). This procedure was performed as previously described by Cullinane et al. (2002). Polarized light micrographs were taken from
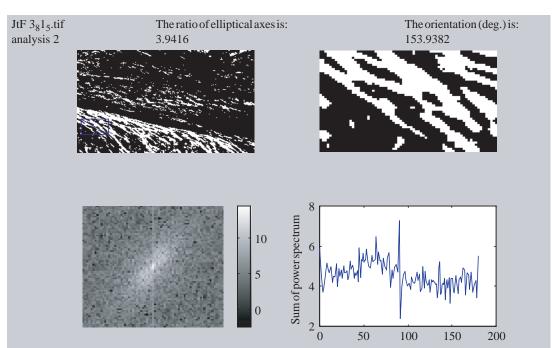
JtF 3_81_5.tif
analysis 2

The ratio of elliptical axes is:
3.9416

The orientation (deg.) is:
153.9382

Fig. 4. An example Fourier transform of collagen fibril architecture. The panels represent the stages of Fourier analysis including a thresholded image, ellipse and frequency distribution. The transform identifies the predominant pattern angle within an image (in this case, fibrillar orientation). The predominant angle, identified by highest frequency, is relative to the original captured image's orientation, but in the final analysis the angle is relative to a presumed defect midline, perpendicular to the bone long axis.

predetermined superficial, intermediate and deep regions of the experimentally derived cartilage tissues in order to highlight collagen fibrils. These images were then incorporated into a Matlab Fourier transform analysis to determine mean collagen fibril orientation and fibrillar agreement (Cullinane et al., 2002).

Molecular analyses

Molecular analyses of the expression of specific genes or proteins was carried out by *in situ* hybridization and immunostaining in order to confirm tissue types and to identify expression of the growth and differentiating factor 5 (GDF-5), respectively. *In situ* hybridization was carried out for collagen type II using a commercially available probe for RNA labeling. Linearized plasmids containing this gene were purchased from Pharmigen Corp. (San Diego, CA, USA). Single stranded ^{35}S-labeled cRNA probes were generated by *in vitro* transcription (Pharmigen Corp.). Linearized plasmids containing each of the selected genes for analysis were transcribed using [^{35}S]uridine triphosphate ([^{35}S]UTP; NEN Life Science Products, Inc., Boston, MA, USA) and T7 RNA polymerase, then digested with DNase, phenol extracted and ethanol precipitated. The labeling efficiency for the cRNA products was determined by scintillation counting and adjusted to a concentration of 3×10^5 c.p.m. μl^{-1} of probe for each *in situ* assay.

Tissue procurement

Tissue samples were fixed overnight in freshly prepared 4% paraformaldehyde at 0°C, followed by decalcification in 14% EDTA for up to eight weeks. Decalcified samples were paraffin embedded.

Tissue preparation and sectioning

Fixed and decalcified tissues were dehydrated in graded ethanol up to 100%, transferred to xylenes, then embedded in paraffin. 5 μm-thin paraffin sections were placed on poly L-lysine-coated slides, dried overnight and used immediately or stored at 4°C.

Probe preparation

Sense and antisense ^{35}S-labeled cRNA probes were used for hybridization. Vectors were appropriately linearized and incubated with either T7 or SP6 RNA polymerase in the presence of [^{35}S]UTP, unlabeled nucleotides, 10 mmol l^{-1} dithiothreitol (DTT) and RNasin RNase inhibitor (Promega, Madison, WI, USA). Labeled cRNA probes were separated from free nucleotides using a Mini Quick Spin RNA column (Roche Molecular Biochemicals, Indianapolis, IN, USA).

Prehybridization

Slides were deparaffinized in xylenes followed by rehydration in graded ethanol solutions, rinsed in 0.85% NaCl (5 min) and 1× phosphate-buffered saline (PBS; 5 min). Sections were treated with proteinase K (20 μg ml^{-1}) for 8 min at 37°C. Slides were dipped successively in 1× PBS (5 min), 4% paraformaldehyde (5 min), acetylated in 0.25% acetic anhydride. GDF-5 expression was examined by immunohistochemistry. For these studies, an antibody to GDF-5 was obtained from Santa Cruz Biotechnology, Inc. (Santa Cruz, CA, USA). Briefly, histochemical staining was carried out using antigen retrieved at 199°F for 10 min in 10 mmol l^{-1} sodium citrate. The anti-GDF-5 antibody (0.5 μg ml^{-1}) was applied to the sections, followed by a biotinylated
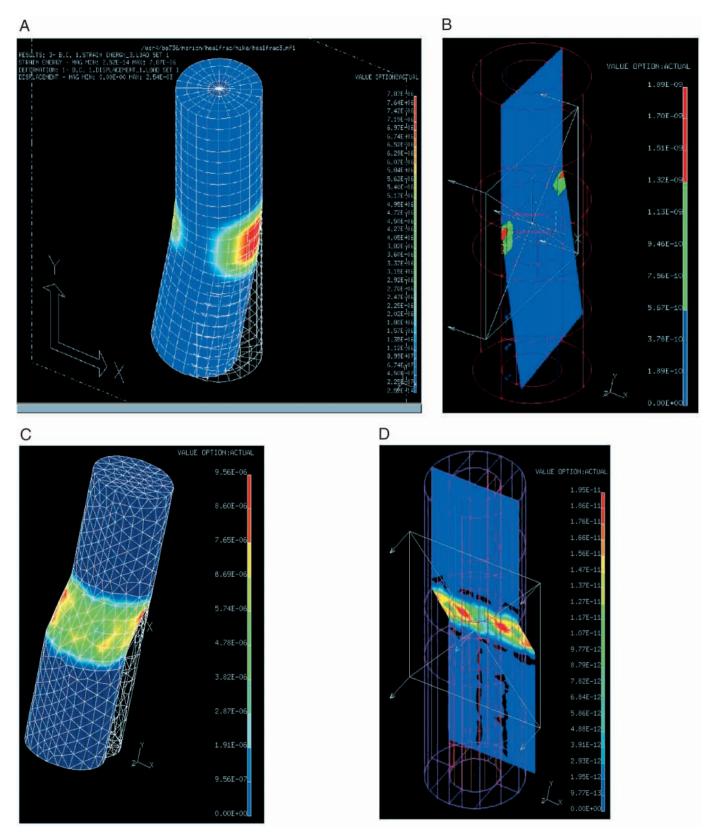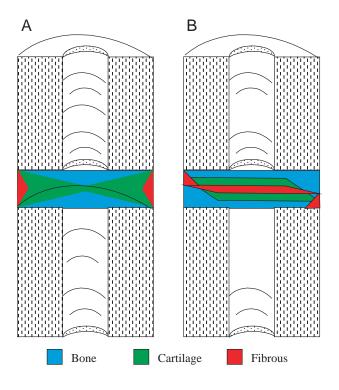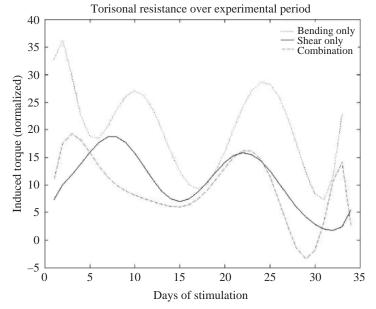
Fig. 5. Finite element models (FEMs) illustrating strain distribution within the defect for shear (A,B) and bending (C,D). The three-dimensional models are to the left (A,C), while their respective cross-section representations are to the right (B,D). The models presented are from an intermediate stage of loading to illustrate the strain progression. The distribution of strain is illustrated using the quantitative color bars to the right of each active model. Altering the mechanical properties of the defect tissues alters the results of the models. The number of brick elements and the composition of the structure also play a role in determining the model's effectiveness in estimating local mechanical loads.

secondary antibody and horseradish peroxidase (HRP)-conjugated streptavidine complex, and visualized with DAB chromogen.

Statistical analysis

Data are presented as means ± S.D. All histomorphometric results, including collagen preferred fiber angle and fiber angle conformity, were compared between the control and treatment groups using analysis of variance (ANOVA) and Tukey's *post-hoc* test at an α level of 0.05, with *P* values of <0.05 interpreted as significant. All sample sizes for the specific groups were determined by power statistics calculations: based on a

Fig. 6. Graphic stress- and strain-based tissue prediction diagrams created from finite element results for (A) 12° bending and (B) shear. The areas in green represent putative cartilage, the areas in red represent fibrous tissues, and the blue areas represent bone. The bending model predicts two opposing bone elements but does not predict that the cartilage element will completely segment between the proximal and distal halves. The shear model predicts cartilage segmentation between the halves.

coefficient of variation of 25% in the data and accepting α and β errors of 5.0%.

Results

Finite element models

The results of the FEMs indicated unique distributions of stress and strain between the bending and shear groups (Fig. 5). The distribution of tensile strain within the bending defect peaked at the defect periphery and subsided linearly in the direction of the defect center. In the bending model, the compressive stresses acted in opposite response to the tensile strain, peaking almost simultaneously but in the vicinity of the opposite cortex. The peak strain levels corresponded with the magnitude of displacement of the cortices on the tensile side during bending excursion. The distribution of compressive stress spanned the entire bending defect, with diminishing values approaching the defect center.

Peak strain levels in the bending group reached 7.87×10^{-6}, while peak strain in the shear groups reached only 1.95×10^{-11}, with a more narrow range of strain distribution in the proximal–distal direction. According to the MFM based on Carter et al. (1988), fibrous tissues would form in the bending group within the estimated range of 7.87×10^{-6} to 6.07×10^{-6}, with cartilage forming in the range from 5.84×10^{-6} to 3.37×10^{-6} and bone within the range from 2.70×10^{-6} to 2.20×10^{-6}. The shear group tissue differentiation ranges for strain include 1.95×10^{-11} to 1.56×10^{-11} for fibrous tissue, 1.47×10^{-11} to 8.79×10^{-12} for cartilage and 7.82×10^{-12} to 2.93×10^{-12} for bone.

The stress and strain distributions were then incorporated into graphic models of expected tissue differentiation for each of the mechanical stimulations (Fig. 6). The graphic model predictions were based on the stress and strain results from the FEMs, interpreted by the MFM. The areas of higher compressive stress were predicted to encourage cartilage differentiation whereas the areas of extreme

Fig. 7. Moment resistance data for bending, shear and combination loading. The bending (dotted line), shear (solid line) and combination (dashed line) data correlate highs and lows very well, except for an initial lag in the combination group. Tissue appearance seems constrained by the timing of physiological processes and mechanobiological principles, while the architecture and maintenance of tissues seems to be controlled primarily by the mechanical environment. Note how the timing of the peaks and troughs correlates well among the three treatment regimens, while the magnitude of the moment resistance varies by treatment.
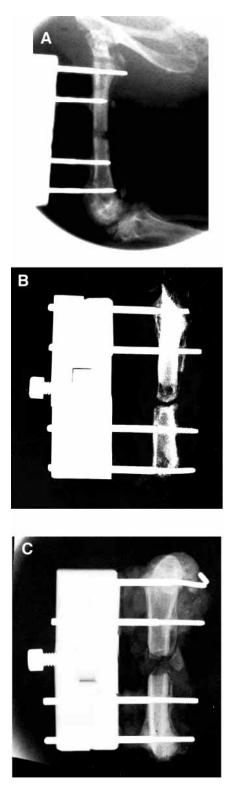
Fig. 8. Radiographs of (A) control, (B) bending and (C) shear specimens with the external fixators attached. In every case, the mechanically stimulated defects resulted in non-union. The cartilage tissues in the experimental treatment defects are represented by translucencies in the gaps between the segments. All experimental treatments were for a 35-day (six-week) duration. The control specimen example is from a four-week control specimen, demonstrating the rapid bony bridging occurring in the controls.

tensile strain were predicted to promote the differentiation of fibrous tissue. The areas within the high compressive stress region but that are shielded by previous cartilage formation are predicted to foster bone. These areas of subchondral bone were predicted to form arch-like structures, peaking at the neutral axis of bending.

Moment analysis

Fig. 7 details the results of the moment analysis for the three mechanical stimulation regimens for the entire 35-day stimulation period, normalized to the stimulation device without an animal attached. ANOVA found a significant difference among the groups ($P<0.001$, $N=4$), with the bending group being significantly different from both the shear and combination groups. The bending group experienced the greatest moment resistance, followed by the shear and combination groups. After initial fluctuations, the three groups appeared to cycle together, with some temporal offset initially in the combination group, and with a magnitudinal difference in the bending group. The bending and combination groups experienced an initial peak at approximately 8–10 days following the onset of stimulation. This peak was followed by a day 15–17 mutual low for all three groups. A subsequent mutual peak at days 23–25 then followed for all three groups, followed by a mutual low at days 30–32. The day 10 peak coincides with the maturation and peak of the cartilaginous stage of callus healing.

Radiology

The weekly radiographs illustrated the onset of bony bridging across the defects in the control specimens, while the treatment defects each demonstrated defect translucency and complete non-union in all specimens (Fig. 8). Areas of reduced density represent cartilage or fibrous tissue, while high-density areas represent mineralized tissues such as bone. A distinctive arch-shaped structure spanning the defect cortices can be seen in several of the bending group specimens.

General histology

The shear treatment was preceded by an experimental test to determine an appropriate shear magnitude. This test, using two shear magnitudes, demonstrated two completely different tissue outcomes. One group experienced 10% shear magnitude while the other experienced 25% shear. The 10% magnitude shear group developed a cartilage band across the entire defect, while the 25% shear defect developed only fibrous tissue across the defect (Fig. 9).

The mechanical treatment groups all demonstrated the presence of a cartilage band spanning the entire defect, while the control specimens demonstrated bony bridging of the defect (Fig. 10). The cartilage tissues stained red while the bone and fibrous tissues stained blue-green. The bending specimens acquired an arched appearance to their cartilage and the underlying subchondral bone arch on at least one side of the defect, while the shear and combination groups showed parallel and evenly distributed cartilage bands.
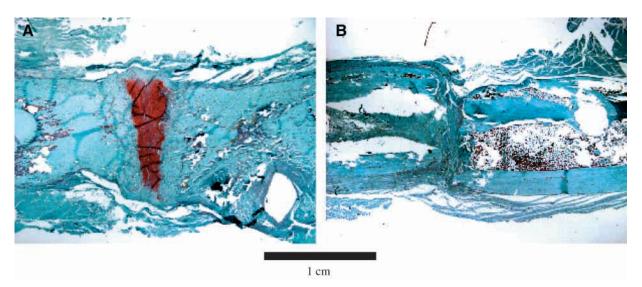
Fig. 9. An illustrative example of the mechanobiological paradigm's predictive value. Here, the magnitude of strain graphically dictates the differentiation of cartilage (shown in red) *versus* fibrous tissue (shown in blue) within the mechanically stimulated defects. The defect shown in A underwent 10% cortex diameter shear, whereas the defect shown in B underwent 25% shear. Thus, a threshold exists between these shear magnitudes that determines cartilage *versus* fibrous tissue outcomes.

Histomorphometrics

Tissue type composition

We found that the ratio of cartilage to bone in our experimental tissues was very similar to that in articular cartilage, especially in comparison with control endochondral healing callus (Table 1). The mean control ratio of bone to cartilage was 94:6. In the experimental results, the mean bending group ratio of bone to cartilage was 78:22 and the shear group was 80:20. The mean combination group ratio was 82:18. None of the treatment groups were significantly different from the knee joint but all were significantly different from the control (*P*<0.05, *N*=4 per group). Thus, we found consistent ratios of cartilage to bone in our experimental tissues, and these mirrored the knee joint mean of roughly 80:20. The intervertebral joint was unique in that its cartilage to bone ratio was significantly different from all others (*P*<0.00062), approximating 50:50.

Collagen architecture quantification

The experimentally generated cartilage tissues demonstrated visually distinct zones of collagen fibril organization with specialized fiber orientations in each zone (Fig. 11). Obvious were the superficial and deep zones, with a less obvious transitional intermediate zone. Mean collagen fibril angles were not significantly different among the different treatment groups for each of the layers, with the exception of the shear intermediate
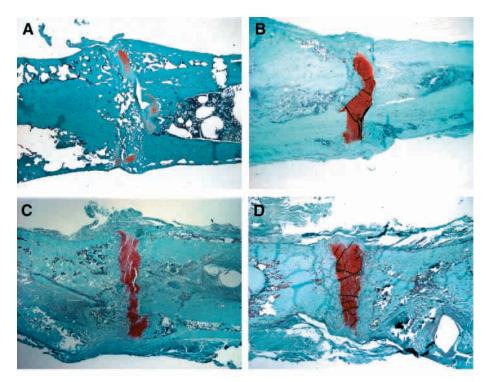

Fig. 10. The histological results from (A) control, (B) bending, (C) bending and shear, and (D) shear stimulations. Note that the control exhibits very little cartilage, while the treatment groups all present cartilage bands (shown in red) spanning the defect. Note also the arched nature of the cartilage band in the bending specimen, a further mechanobiological response to the bending action.

fiber1.tif
Analysis 1

The ratio of elliptical axes is:
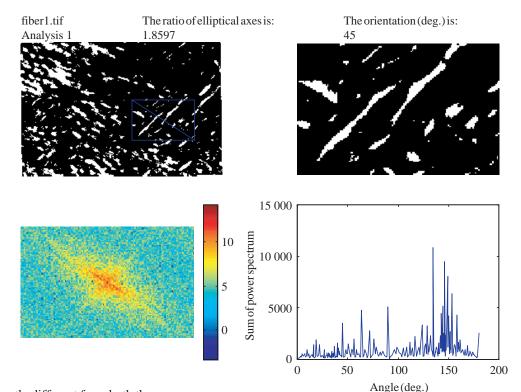1.8597

The orientation (deg.) is:
45

Fig. 11. Fourier transformation of control cartilage collagen fibril orientation. The control cartilage collagen is randomly oriented due to a small-magnitude, unpredictable loading environment. Very little cartilage is produced within the control specimens due to rigid fixation.

layer (Table 2), which was significantly different from both the bending and combination groups ($P<0.001$, $N=4$ per group). The intervertebral joint tissue was not used in this analysis due to its specialized structural configuration.

Molecular analysis

In situ hybridization confirmed the presence of type II collagen within the tissues differentiating in the experimental defects (Fig. 12). Type II collagen is a marker molecule for all forms of cartilage, and its presence confirms that the tissue differentiating within the defect is cartilage. We observed collagen type II expression at constant but relatively low levels throughout the tissue. However, higher levels of expression were seen in a band of cells adjacent to the area of fibrous tissue where cartilage cavitation was initiating (Fig. 12A). We also saw a weaker band of labeled cells adjacent to the subchondral bone formed under the cartilage band. Immunohistology also identified the presence of growth and differentiating factor 5 (GDF-5) within the cells of the bending experimental cartilage (Fig. 13). The positive presence of this
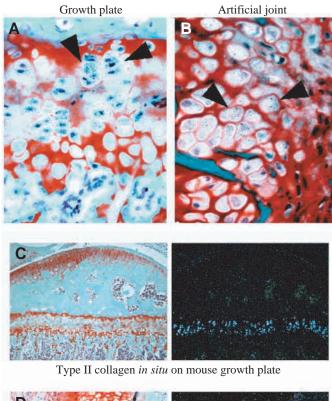
Table 1. *Tissue type composition*

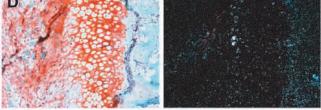| Category	% Bone (mean ± S.D.)	% Cartilage (mean ± S.D.)
Control	94.27±4.11	5.73±4.80
Bending	78.40±2.63	21.57±2.60
Shear	80.18±5.78	19.82±3.03
Combination	81.89±13.17	18.11±13.15
Native knee	83.57±1.88	16.43±2.64
Native intervertebral	53.87±13.02	46.13±7.53

The results of the three treatment groups – bending, shear, and combination – are compared with those of the control group and native knee joint. The three treatment groups approximate the 80:20 bone to cartilage ratio found in the knee joint, while the mean control group ratio of bone to cartilage is 94:6. The mean intervertebral joint ratio of bone to cartilage is 50:50.

Table 2. *Collagen architecture quantification*

	Mean collagen fibril angles (deg.)				
	Control	Articular cartilage	Bending	Shear	Combination
Superficial	101.67±105.7	4.62±4.1	10.68±5.1	5.41±1.5	9.85±4.9
Intermediate	35.89±12.7	17.37±11.2	24.04±7.5	11.41±3.6*	32.35±15.6
Deep	76.65±82.2	92.79±34.9	62.99±21.1	91.66±16.7	83.51±19.3

The results from the three treatment groups are compared with those of the knee articular cartilage. The only significant difference between the groups is the shear intermediate result *versus* the other intermediate values ($P<0.05$; shown by an asterisk). The three treatment groups approximate the collagen fibril angles found in articular cartilage, while the controls demonstrate random angularity.

Growth plate　　　　　Artificial joint

Type II collagen *in situ* on mouse growth plate

Type II collagen *in situ* on rat artificial joint

Fig. 12. *In situ* hybridization analysis of type II collagen mRNA expression in control murine femoral joint tissues and in mechanically induced tissues. (A) 10× magnification analysis comparing light- and dark-field images of *in situ* hybridization profiles of a normal murine joint and the underlying epiphyseal plate. Note the intense primary expression of type II collagen in the epiphyseal plate but not in the area of mature joint cartilage collagen. The black arrowheads in A and B indicate expression of Type II collagen. (B) 20× magnification analysis of the cartilage tissue produced by controlled mechanical loading, forming an artificial joint-like structure. Collagen type II expression is seen at low levels throughout the tissue but shows higher levels of expression in a band of cells adjacent to the area of fibrous tissue where cartilage cavitation is beginning to occur. (C) The 40× magnification shows silver grain localization over cartilage cells of native cartilage within the epiphysis and (D) over chondrocytes within mechanically generated tissues.

molecule is indicated by a brown stain located around the cells differentiating within the defect. Its presence in the experimental tissues is contrasted by its absence in the controls.
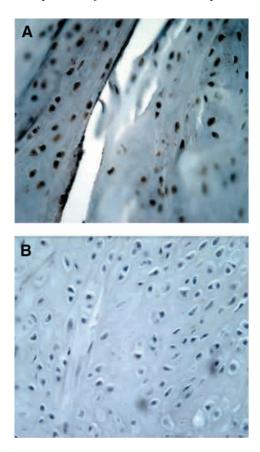

Fig. 13. Immunohistologically stained sections of (A) bending-stimulated and (B) control cartilages. The brown stain in the mechanically stimulated cartilage indicates the expression of growth and differentiating factor 5 (GDF-5), whereas the control section demonstrates no reaction. The positive reaction to GDF-5 indicates that the mechanical stimulation therapy is causing the expression of this joint-determining gene.

Discussion

The results of this study confirm that an empirical relationship exists between the mechanical environment and gene expression, tissue formation and tissue architecture within a mechanically stimulated healing bone defect. The analyses of tissue types and their molecular architecture verify that mechanical intervention influences tissue repair and that some aspects of early development can be recapitulated within a healing adult defect. It also suggests that the repair process for virtually all skeletal tissues can be manipulated towards desirable outcomes based on precise mechanical intervention.

The FEMs accurately predicted the production and persistence of cartilage within the defects and went as far as to predict the presence of fibrous tissues in specific areas of both the bending and shear models. The mechanical stimulations created uniform cartilage bands across the entire defects that persisted well past the timeframe of bony bridging found in the controls. The bending model predicted the presence of stress and strain distributions, peaking in the center of the defect and diminishing toward the cortices. These distributions resulted in

an arch-like bony structure forming across the medullary canal in the bending specimens. The results of the shear pilot study are particularly interesting because they underline the extremely divergent tissue types one can expect based solely on differences in the magnitude of the local mechanical environments. These results in particular serve as a potent example of the predictive power of the mechanobiological paradigm.

The moment resistance data is interesting because it appears to coincide with tissue developmental timing events such as the onset of cartilage formation (15–20 days post-surgery) and perhaps even the formation of ligament-like connective tissues on the periphery of the defect. Tissue segmentation events (chiefly cartilage) probably resulted in the steep declines in moment resistance following the day 10 and day 25 peaks, while connective tissue formations such as ligament-like tissues probably resulted in increases in moment resistance. The magnitude of moment resistance is probably related to the mechanics of bending *versus* shear and, specifically, the extreme tension and compression generated *via* bending. This information goes far in explaining the significant difference in the bending group data. The individual highs and lows are probably related to the tissue types being formed within the defects, and thus are time-dependent as well as mechanobiologically dependent. Thus, the appearance of a tissue is constrained by time and physiological processes as well as by mechanobiological principles, while the architecture and maintenance of a tissue is related more to the mechanical environment.

The histomorphometric results verify that the ratio of cartilage to bone within the experimentally treated defects is in large part controlled by mechanics. The collagen fibrils within the experimentally derived tissues demonstrate organized patterns that resemble those found in articular cartilage. Finally, specific mechanical stimuli can trigger the expression of the genes encoding collagen type II (cartilage formation) and GDF-5 (bone and joint formation). These results further suggest that induced mechanical stimulation during the process of bone defect repair can cause a recapitulation of developmental events from joint formation. It is interesting to note that during stable fracture repair, *GDF-5* expression appears in a tightly defined window during the endochondral phase of fracture and disappears as soon as bone replacement is initiated (Cho et al., 2002). Such results suggest that in the absence of continued mechanical intervention, the expression of this gene is downregulated and would further suggest that it plays an important role either in the maintenance of cartilage or in the retardation of further endochondral maturation. It may reflect the possibility that the experimentally induced activity of this gene is a vestigial attribute of the mechanisms of original joint formation.

Our molecular results are encouraging because they demonstrate two principal findings: first, the presence of collagen type II confirms that our experimentally derived tissues are true cartilage and, second, a gene associated with the *in utero* development of joints (*GDF-5*) is upregulated as a result of the bending stimulation (Storm and Kingsley, 1999). The comparison between the *in situ* reactions in normal postnatal long bones and those obtained from the mechanically induced cartilage was very informative. High levels of cartilage mRNA expression were not observed in fully differentiated joint tissues but were observed with very intensely labeled areas of cartilage formation within the epiphyseal growth plate. Similarly, in the areas of mechanically induced cartilage formation we observed collagen type II expression at low levels throughout the tissue. However, higher levels of expression were seen in a band of cells adjacent to the area of fibrous tissue where cartilage cavitation was initiating. We also saw a weaker band of labeled cells adjacent to the subchondral bone that formed under the cartilage band. These results suggest that the mechanical environment has a direct and quantifiable effect on gene expression and tissue differentiation within healing bone defects.

The origin of the cells that populate the defect following the surgical procedure and during the duration of the experiment is an intriguing question. Very little is known about the precise origin of the cells invading the callus during the many stages of defect repair (Denker et al., 2001; Hunziker et al., 2001; O'Driscoll and Fitzsimmons, 2001). The hematoma probably arises from vascular cells that invade the defect and fill the gap, while cells that form the cartilage tissue originate from the periosteum (Denker et al., 2001; Hunziker et al., 2001; O'Driscoll and Fitzsimmons, 2001). In bone formation, cells must invade from the marrow as they do during initial endochondral bone formation. The origin of the cells within the defect may be academic since it seems that the local mechanical environment can regulate and direct their maturation trajectory to mature cells.

Finally, the experimentally generated tissues and their molecular architecture took on joint-like characteristics in several aspects of our analyses. This is an intuitive outcome in our estimation, as the mechanical interventions were designed to mimic the actions of a developing joint. These results emphasize, on numerous levels, the importance of the mechanical environment in tissue differentiation during both development and repair. It should also be noted that cases of mechanically unstable fractures will likewise demonstrate the presence of cartilage within a healing bone defect, but the location, amount and architecture of that cartilage differs markedly from our precisely mechanically generated cartilages. A classic pseudoarthrosis or 'false joint' is typically a random conglomeration of fibrotic tissue, cartilage and bone. This configuration is directly related to the random instability of the local mechanical environment and its variant magnitudes.

The outcomes of this study confirm that mechanobiological principles can accurately predict gene expression, tissue differentiation and tissue architecture based on manipulations of the local mechanical environment during healing. The results further emphasize the important role the local mechanical environment plays in the everyday development

and repair of the vertebrate body. Further studies need to be conducted in order to determine the precise relationships between the physical environment and gene expression, tissue development and tissue repair.

References

Athanasiou, K. A., Rossenwasser, M. P., Buckwalter, J. A., Malini, T. I. and Mow, V. C. (1991). Interspecies comparison of in situ intrinsic mechanical properties of distal femoral cartilage. *J. Orthop. Res.* **9**, 330-340.

Beaupre, G. S., Stevens, S. S. and Carter, D. R. (2000). Mechanobiology in the development, maintenance, and degeneration of articular cartilage. *J. Rehabil. Res. Dev.* **37**, 145-151.

Carter, D. R. (1987). Mechanical loading history and skeletal biology. *J. Biomech.* **20**, 1095-1109.

Carter, D. R., Blenman, P. R. and Beaupre, G. S. (1988). Correlations between mechanical stress history and tissue differentiation in initial fracture healing. *J. Orthop. Res.* **6**, 736-748.

Carter, D. R., Wong, M. and Orr, T. E. (1991). Musculoskeletal ontogeny, phyology, and functional adaptation. *J. Biomech.* **24**, 3-16.

Carter, D. R., Beaupre, G. S., Giori, N. J. and Helms, J. A. (1998a). Mechanobiology of Skeletal regeneration. *Clin. Orthop.* **355**, S41-S55.

Carter, D. R., van der Meulen, M. C. H. and Beaupre, G. S. (1998b). Mechanobiologic regulation of osteogenesis and athrogenesis. In *Skeletal Growth and Development: Clinical Issues and Basic Science Advances* (ed. J. A. Buckwalter, M. G. Ehrlich, L. J. Sandell and S. B. Trippel), pp. 99-130. Rosemont, IL: American Academy of Orthopedic Surgery.

Carter, D. R. and Beaupre, G. S. (2001). Skeletal tissue histomorphometry and mechanics. In *Skeletal Function and Form* (ed. D. R. Carter and G. S. Beaupre), pp. 31-52. Cambridge: Cambridge University Press.

Cho, T.-J., Gerstenfeld, L. C. and Einhorn, T. A. (2002). Differential temporal superfamily during murine fracture expression of members of the TGF-beta healing. *J. Bone Min. Res.* **17**, 513-520.

Claes, L., Eckert-Hubner, K. and Augat, P. (2002). The effect of mechanical stability on local vascularization and tissue differentiation in callus healing. *J. Orthop. Res.* **20**, 1099-1105.

Claes, L. E. and Heigele, C. A. (1999). Magnitudes of local stress and strain along bony surfaces predict the course and type of fracture healing. *J. Biomech.* **32**, 255-266.

Cullinane, D. M., Inoue, N., Meffert, R., Tis, J., Rafiee, B. and Chao, E. Y. S. (1999). Regulating bone at the cellular level: a little evidence for Wolff's Law. *Am. Zool.* **39**, 96.

Cullinane, D. M., Fredrick, A., Eisenberg, S. R., Pacicca, D., Elman, M. V., Lee, C., Salisbury, K. Gerstenfeld, L. C. and Einhorn, T. A. (2002). Induction of articular-like cartilage and a joint-like structure by controlled motion in an experimental mid-femoral defect. *J. Orthop. Res.* **20**, 579-586.

Denker, A. E., Van Rheeden, R., Watson, M. and Sandell, L. J. (2001). Bone marrow cell distribution during early fracture healing. 47th Ann. Meet. Orthop. Res. Soc., San Francisco.

de Rooji, P. P., Siebrecht, M. A., Tagil, M. and Aspenberg, P. (2001). The fate of mechanically induced cartilage in an unloaded environment. *J. Biomech.* **34**, 961-966.

Eckstein, F., Faber, S., Muhlbauer, R., Hohe, J., Englmeier, K. H., Reiser, M. and Putz, R. (2002). Functional adaptation of human joints to mechanical stimuli. *Osteoarthr. Cart.* **10**, 44-50.

Elder, S. H., Goldstein, S. A., Kimura, J. H., Soslowsky, L. J. and Spengler, D. M. (2001). Chondrocyte differentiation is modulated by frequency and duration of cyclic loading. *Ann. Biomed. Eng.* **29**, 476-482.

Ferguson, C., Alpern, E., Miclau, T. and Helms, J. A. (1999). Does adult fracture recapitulate embryonic skeletal formation? *Mech. Dev.* **87**, 57-66.

Gardner, T. N., Stoll, T., Marks, L., Mishra, S. and Tate, M. K. (2000). The influence of mechanical stimulus on the pattern of tissue differentiation in a long bone frature – a FEM study. *J. Biomech.* **33**, 415-425.

Giori, N. J., Beaupre, G. S. and Carter, D. R. (1993). Cellular shape and pressure may mediate mechanical control of tissue composition in tendons. *J. Orthop. Res.* **11**, 581-591.

Grodzinsky, A. J., Leveston, M. E., Jin, M. and Frank, E. H. (2000). Cartilage tissue remodeling in response to mechanical forces. *Annu. Rev. Biomed. Eng.* **2**, 691-713.

Hall, B. K. (1972). Immobilization and cartilage transformation into bone in the embryonic chick. *Anat. Rev.* **173**, 391-403.

Hartmann, C. and Tabin, C. J. (2001). Wnt-14 plays a pivotal role in inducing synovial joint formation in the developing appendicular skeleton. *Cell* **104**, 341-351.

Heegaard, J. H., Beaupre, G. S. and Carter, D. R. (1999). Mechanically modulated cartilage growth may regulate joint surface morphogenesis. *J. Orthop. Res.* **17**, 509-517.

Hunziker, E. B., Driesang, I. M. K. and Morris, E. A. (2001). Experimental models of cartilage repair: chondrogenesis in cartilage repair is induced by members of the transforming growth factor-beta superfamily. *Clin. Orthop. Rel. Res.* **391** (suppl.), S171-S181.

Loboa, E. G., Beaupre, G. S. and Carter, D. R. (2001). Mechanobiology of initial pseudoarthrosis formation with oblique fractures. *J. Orthop. Res.* **19**, 1067-1072.

Loboa-Polefka, E. G., Wren, T. A. L. and Carter, D. R. (2002). Mechanobiology of soft tissue regeneration. 48th Annual Meeting Orthop. Res. Soc., Dallas.

O'Driscoll, S. W. and Fitzsimmons, J. S. (2001). Experimental models of cartilage repair: the role of periosteum in cartilage repair. *Clin. Orthop. Rel. Res.* **391** (suppl.), S190-S207.

Sarin, V. K. and Carter, D. R. (2000). Mechanobiology and joint conformity regulate endochondral ossification of sesamoids. *J. Orthop. Res.* **18**, 706-712.

Smith, R. L., Thomas, K. D., Schurman, D. J., Carter, D. R., Wong, M. and van der Meulen, M. (1992). Rabbit knee immobilization: Bone remodeling precedes cartilage degredation. *J. Orthop. Res.* **10**, 88-95.

Smith-Adaline, E. A., Ignelzi, M. A., Volkman, S. K., Slade, J. M. and Goldstein, S. A. (2002). Chondrogenesis is influenced by mechanical environment during fracture healing concommitant with altered expression of BMP-4, VEGF, and IHH. 48th Annual Meeting Orthop. Res. Soc., Dallas.

Storm, E. E. and Kingsley, D. M. (1999). GDF-5 coordinates bone and joint formation during digit development. *Dev. Biol.* **209**, 11-27.

van der Meulen, M. C., Beaupre, G. S. and Carter, D. R. (1993). Mechanobiologic influences in long bone cross-sectional growth. *Bone* **14**, 635-642.

van der Meulen, M. C., Morey-Holton, C. R. and Carter, D. R. (1995). Hindlimb suspension diminishes femoral cross-sectional growth in the rat. *J. Orthop. Res.* **13**, 700-707.

van der Meulen, M. C. H. and Carter, D. R. (1995). Developmental mechanics determine long bone geometry. *J. Theor. Biol.* **172**, 323-327.

van der Meulen, M. C. H. and Huiskes, R. (2001). Why mechanobiology? *J. Biomech.* **35**, 401-414.

Waanders, N. A., Richards, M., Steen, H., Kuhn, J. L., Goldstein, S. A. and Goulet, J. A. (1998). Evaluation of the mechanical environment during distraction osteogenesis. *Clin. Orthop.* **349**, 225-234.

Whalen, S. (1993). Musculoskeletal adaptation to mechanical forces on Earth and in space. *Physiologist* **36**, S127-S130.

Wolff, J. (1892). *Das Gaesetz der Transformation der Knochen* (ed. A Hirchwald). Berlin.